24-nt phasiRNAs move from tapetal to meiotic cells in maize anthers

Xue Zhou[1*], Kun Huang[2,3,4], Chong Teng[5], Ahmed Abdelgawad[6], Mona Batish[6,7], Blake C. Meyers[5,8] and Virginia Walbot[1]

[1]Department of Biology, Stanford University, Stanford, CA 94305, USA; [2]Department of Plant and Soil Sciences, University of Delaware, Newark, DE 19716, USA; [3]Delaware Biotechnology Institute, University of Delaware, Newark, DE 19716, USA; [4]Dana-Farber Cancer Institute Molecular Imaging Core, 360 Longwood Ave, MA, 02215, USA. [5]Donald Danforth Plant Science Center, St. Louis, MO 63132, USA; [6]Department of Biological Sciences, University of Delaware, Newark, DE 19716, USA; [7]Department of Medical and Molecular Sciences, University of Delaware, Newark, DE 19716, USA; [8]Division of Plant Sciences, University of Missouri – Columbia, Columbia, MO 65211, USA

[*]**Author for correspondence:**
Xue Zhou
Tel: +1-530-760-5689
Email: xuezhouxz@gmail.com

Total word count for the main body of the text (Introduction, Materials and Methods, Results, Discussion): 5590
No. of Summary: 145
No. of Introduction: 972
No. of Materials and Methods: 1298
No. of Results: 2219
No. of Discussion: 1101
No. of Acknowledgments: 93
No. of Author contributions: 63
No. of Figures: 5 (Fig.1-5 in color)
No. of Tables: 0
No. of Supporting Information files: 16 (Fig. S1-S10 in color; Table S1-S6)

Summary

- In maize, 24-nt phased, secondary small interfering RNAs (phasiRNAs) are abundant in meiotic stage anthers, but their distribution and functions are not precisely known.
- Using laser capture microdissection, we analyzed tapetal cells, meiocytes, and other somatic cells at several stages of anther development to establish the timing of 24-*PHAS* precursor transcripts and the 24-nt phasiRNA products.
- By integrating RNA and small RNA profiling plus single-molecule and small RNA FISH (smFISH or sRNA-FISH) spatial detection, we demonstrate that the tapetum is the primary site of 24-*PHAS* precursor and *Dcl5* transcripts and the resulting 24-nt phasiRNAs. Interestingly, 24-nt phasiRNAs accumulate in all cell types, with the highest levels in meiocytes, followed by tapetum.
- Our data support the conclusion that 24-nt phasiRNAs are mobile from tapetum to meiocytes and to other somatic cells. We discuss possible roles for 24-nt phasiRNAs in anther cell types.

Key words: *Zea mays* (maize), laser capture microdissection, smFISH/sRNA-FISH, 24-nt phasiRNA, mobility

50 **Introduction**

51 In plants, small RNAs (sRNAs) belong to three main categories: microRNAs (miRNAs)
52 involved in target mRNA cleavage, heterochromatic small interfering RNAs (hc-siRNAs)
53 involved in RNA-directed DNA methylation (RdDM), and phased, secondary small interfering
54 RNAs (phasiRNAs). PhasiRNAs were initially reported in male reproductive organs of maize
55 and rice (Johnson *et al.*, 2009; Song *et al.*, 2012a; Zhai *et al.*, 2015; Fei *et al.*, 2016; Tamim *et*
56 *al.*, 2018; Teng *et al.*, 2020), and more recently in diverse monocots and eudicots (Kakrana *et al.*,
57 2018; Xia *et al.*, 2019; Patel *et al.*, 2021; Pokhrel *et al.*, 2021); they are found primarily in
58 anthers. In most species, 21-nt phasiRNAs predominate during early anther development, while
59 24-nt phasiRNAs are abundant during meiosis.

60 PhasiRNA biogenesis starts with transcription of long noncoding precursors (*PHAS*
61 transcripts) by RNA polymerase II. Subsequently, the *PHAS* transcripts are capped and
62 polyadenylated, translocated to the cytoplasm, and then bound by ribosomes (Yang *et al.*, 2021).
63 In the polysomal complex, an Argonaute-associated 22-nt miRNA complementary to sequences
64 in the *PHAS* transcript binds to this precursor molecule and triggers cleavage. miR2118 is
65 utilized for most 21-nt *PHAS* precursors and miR2275 for most 24-nt *PHAS* precursors based on
66 the presence of complementary sequences; a fraction of precursors lacks such complementarity
67 and may be processed utilizing other miRNAs. Then, the 3′ portions of cleaved transcripts are
68 converted to double-stranded RNA by RNA-DEPENDENT RNA POLYMERASE 6 (RDR6),
69 and subsequently processed by Dicer-like proteins (DCL4 for the 21-nt and DCL5 for the 24-nt
70 type) to yield the phasiRNAs (Song *et al.*, 2012a; Song *et al.*, 2012b; Zhai *et al.*, 2015; Teng *et*
71 *al.*, 2020). Despite the expectation of equal stoichiometry of all the products from one *PHAS*
72 transcript, individual phasiRNA abundances derived from the same transcript can differ by more
73 than 1000-fold indicating differential stabilization (Tamim *et al.*, 2018; Zhang *et al.*, 2021). It is
74 possible that only these few abundant products generated from one precursor have functions.

75 In maize the 21-nt phasiRNAs are distributed throughout immature anther lobes based on
76 *in situ* hybridizations with one or a few examples, although the production of miR2118 is
77 restricted to the epidermis (Zhai *et al.*, 2015). Several observations associate phasiRNAs with
78 male sterility. First, the absence of specific 21-nt phasiRNAs are implicated in causing male
79 sterility in rice (Komiya *et al.*, 2014; Fan *et al.*, 2016). Second, in numerous male-sterile mutants
80 of maize, either the 21-nt or 24-nt phasiRNAs are absent reflecting the tight control of the normal

81 timing of their appearance during development (Zhai *et al.*, 2015; Nan *et al.*, 2017; Teng *et al.*,
82 2020; Yadava *et al.*, 2021). More specifically addressing the role of 24-nt phasiRNAs, *dicer-*
83 *like5* mutants unable to process most 24-nt *PHAS* precursors are male-sterile and exhibit aberrant
84 tapetal development under normal growing conditions (Teng *et al.*, 2020). In maize, the
85 expression of *PHAS* precursors and miR2275 as well as the accumulation of 24-nt phasiRNAs
86 occur mainly in the tapetum at the prophase I stage in anthers (Zhai *et al.*, 2015). Male-sterile
87 mutants with tapetal developmental defects evident during early meiotic stages are missing the
88 24-nt phasiRNAs (Nan *et al.*, 2017; Teng *et al.*, 2020). Interestingly, the male sterility cases in
89 rice and maize exhibit temperature-dependent male sterility: in appropriate growing conditions,
90 the plants are male-fertile despite the absence of specific or an entire class of phasiRNAs (Fan *et*
91 *al.*, 2016; Teng *et al.*, 2020; Yadava *et al.*, 2021). This observation has led to the hypothesis that
92 phasiRNAs may buffer anther development against environmental perturbation, particularly in
93 the tapetum. In addition to the expectation that phasiRNAs could modulate mRNA half-life of
94 still poorly defined targets, the 24-nt phasiRNAs result in increased CHH DNA methylation at
95 24-*PHAS* loci in maize, as assessed in whole anthers (Zhang *et al.*, 2021). In analysis of isolated
96 meiocytes, 24-nt phasiRNAs have been detected, and there is an increase in CHH DNA
97 methylation, leading to the hypothesis that these phasiRNAs might regulate meiosis (Dukowic-
98 Schulze *et al.*, 2016) by an unknown mechanism related to *cis* methylation of their own loci. To
99 date, the precise role of 24-nt phasiRNAs in regulating maize anther development has remained
100 elusive.
101 sRNAs can function by travelling within and between organs: from the site of synthesis,
102 they can spread both to neighboring cells and systemically over long distance (Chitwood &
103 Timmermans, 2010; Dunoyer *et al.*, 2010; Molnar *et al.*, 2010). Cell-to-cell movement of sRNAs
104 is probably through plasmodesmata (PD), a plasma membrane-lined pore acting as an
105 intercellular channel that connects the cytoplasm of adjacent cells (Dunoyer *et al.*, 2013). To
106 date, the potential movement of 24-nt phasiRNAs from the site of biogenesis to the neighboring
107 cell layers in maize anthers has not been well studied. A major concern with our previous
108 localization analysis for 24-nt phasiRNAs and biogenesis components primarily to the tapetum is
109 that only a few examples were evaluated, and the probes could adhere to the callose coat
110 surrounding the germinal cells, yielding a non-specific signal (Zhai *et al.*, 2015). Therefore, in
111 meiotic stage maize anthers, two major questions should be addressed: 1) do meiocytes contain

112 all the components for generating 24-nt phasiRNAs? And 2) using RNA-seq and small RNA-seq,
113 what is the timing of synthesis and the distribution of these components in anther lobes?
114 To explore the distribution of 24-nt phasiRNA biogenesis components and the resulting
115 small RNAs, we used laser capture microdissection (LCM) to isolate meiocytes (ME), tapetum
116 (TAP), and other somatic cells (OSC) from two anther developmental stages for low input RNA-
117 seq and sRNA-seq and for a more comprehensive developmental analysis using RT-qPCR. By
118 integrating comprehensive RNA/sRNA profiling and single-molecule or sRNA FISH
119 (smFISH/sRNA-FISH) spatial detection, we demonstrate that TAP contain the most 24-*PHAS*
120 primary transcripts, whereas ME ultimately accumulate more 24-nt phasiRNAs at meiotic
121 prophase I. We discuss these results in a model in which 24-nt phasiRNAs move from TAP to
122 ME during meiosis.

Materials and Methods

Plant material

Maize (*Zea mays*) W23 *bz2* inbred line plants were grown in Stanford, CA, USA under greenhouse conditions (31 °C/21 °C, 14 h day/10 h night light cycle with supplemental LED and UV-A lamps providing ~50% of summer sun conditions). Anthers were dissected from tassels and then measured using a micrometer (Fisher Scientific). Homozygous *dcl5-mu03//dcl5-mu03* plants are temperature-sensitive male sterile. They are male sterile under optimized growth condition (28 °C/22 °C day/night temperature, 14 h light, 400 µmol/m^2/s) in the greenhouse. *dcl5-mu03//dcl5-mu03* male sterile and *dcl5-mu03//Dcl5* fertile siblings were grown in St. Louis, MO, USA under the optimized growth conditions in a greenhouse.

Laser Capture Microdissection (LCM)

Fifty upper floret anthers were dissected from individual central tassel spikes for each biological replicate. Different stage anther samples were collected from different maize plants. ME, TAP, and OSC were isolated from 1.25 mm, 1.5 mm, and 2.0 mm W23 anthers by LCM as described previously (Kelliher & Walbot, 2012), with minor modification. Fixed anthers were cryoprotected in 10% (2-3 days) and 15% sucrose/PBS (phosphate buffered saline) (5 to 7 days) to better preserve tapetal cell layer morphology. Total RNA was isolated from each cell type using the RNAqueous™-Micro Kit (Invitrogen); RNA quality was evaluated on an Agilent Bioanalyzer using the RNA 6000 Pico Kit (Agilent Technologies).

Cytological staging and imaging

AR/PMC/ME from W23 anthers (from the 0.75 mm through 2.25 mm anther length stages, recovered at 0.25 mm intervals) were extruded, classified using a micrometer, and then appropriately sized anthers were stained with 10 µg/mL Hoechst 33342 (Sigma-Aldrich) according to our pervious report (Nelms & Walbot, 2019). Confocal image stacks for the germinal cells were taken with a Leica SP8 microscope using a 93X Glycerol immersion objective. ImageJ (Schneider *et al.*, 2012) was used for processing the fluorescent microscopy images. Cytological stages during meiotic prophase I were assigned using established criteria (Dawe *et al.*, 1994; Nelms & Walbot, 2019).

154 **RNA-seq and sRNA-seq library construction and sequencing**

155 Total RNA was isolated from three different LCM cell samples and FA samples at 1.5 mm and
156 2.0 mm using the RNAqueous™-Micro Kit (Invitrogen). RNA-seq libraries were prepared using
157 CEL-seq2 (Hashimshony *et al.*, 2016) based on a modified protocol (Nelms & Walbot, 2019).
158 Primers were synthesized by phosphoramidite chemistry at the Stanford Protein and Nucleic
159 Acid Facility (Stanford, CA) (Table **S1**). All RNA-seq libraries were sequenced on an Illumina
160 HiSeq 4000 instrument at the Stanford Genome Sequencing Service Center (Stanford, CA) with
161 paired-end 150 bp reads.

162 For small RNA library preparation, RealSeq®-AC kits (SomaGenics) were used for ultra-
163 low amounts of total RNA starting with 100 ng from whole anthers or 10 ng from LCM cell
164 samples. Sequencing in a single-end mode on an Illumina NextSeq (University of Delaware)
165 yielded 75 bp reads for sRNA-seq.

166

167 **Data handling and bioinformatics**

168 Paired-end RNA-seq Read1 contained a 10 bp unique molecular identifier (UMI) (Kivioja *et al.*,
169 2011) and sample barcodes, and Read2 contained the transcript sequence. Each UMI was
170 processed and attached to the Read2 metadata using fastp (Chen *et al.*, 2018). Barcodes were
171 used to demultiplex Read2 into a separate file for each library using fastq-multx (Aronesty,
172 2013). After trimming the adapters by Trim Galore, the reads were mapped to version 4 of the
173 B73 maize genome using Hisat2 (Pertea *et al.*, 2016). RNA-seq reads were normalized by
174 dividing by the total number of transcripts (UMIs) in each sample and multiplying by one
175 million (transcripts per million normalization).

176 sRNA-seq data were processed as previously described (Mathioni *et al.*, 2017). In brief,
177 Trimmomatic version 0.32 (Bolger *et al.*, 2014) was used to remove the linker adaptor
178 sequences. Then, the trimmed reads were mapped to version 4 of the B73 maize genome using
179 Bowtie (Kersey *et al.*, 2016). Read counts were normalized to one million to allow for the direct
180 comparison across libraries. PhasiRNAs were designated based on the criteria of a 24-nt length
181 and mapping coordinates within the previously identified 176 *24-PHAS* loci (Zhai *et al.*, 2015)
182 that were updated to version 4 of the B73 genome using the assembly converter tool (Tello-Ruiz
183 *et al.*, 2018).

184

185 **Quantitative reverse transcription PCR (RT-qPCR)**
186 RT-qPCR for multiple stage anthers (0.75 mm – 2.0 mm; 0.25 mm intervals) and LCM cell
187 sample collections (ME, TAP, and OSC) was performed using the Luna® Universal Probe One-
188 Step RT-qPCR Kit (New England Biolabs). Quantitative PCR was performed using TaqMan
189 primers synthesized by Integrated DNA Technologies (Table **S2**) on a CFX96 C1000 Touch
190 Real-Time PCR Detection System (BioRad). *ZmCyanase* expression was used to normalize
191 among biological samples, because this gene is highly expressed at all stages of anther
192 development (Fig. **S5**). Each sample type was tested in two biological and three technical
193 replicates.
194
195 **Single-molecule fluorescence *in situ* hybridization (smFISH) for mRNAs and sRNAs**
196 Maize spikelets of various sizes were dissected from the central spike and fixed in 20 mL glass
197 vials using 4% paraformaldehyde in 1x PHEM buffer (5 mM HEPES, 60 mM PIPES, 10 mM
198 EGTA, 2 mM $MgCl_2$ pH 7). Fixation was done three times in a vacuum chamber at 0.08 MPa, 15
199 min each. After fixation, samples were sent for paraffin embedding at the histology lab in the
200 Nemours/Alfred I. duPont Hospital for Children (Wilmington, DE). Embedded paraffin samples
201 were sectioned using a paraffin microtome and dried on poly-l-lysine-coated 22 x 22 mm #1.5
202 coverslips (Carl Zeiss Microscopy, LLC, Cat# 474030-9020-000). Samples were then de-
203 paraffinized using Histo-Clear (Fisher Scientific, 50-899-90147) and re-hydrated by going
204 through an ethanol series of 100, 95, 80, 70, 50, 30, 10% (vol/vol) (30 sec each) and finally water
205 (1 min) at room temperature. After protease (Sigma, P5147) digestion (20 min, 37°C), samples
206 were neutralized in 0.2% glycine (Sigma-Aldrich, G8898) for 2 min. After two washes in 1X
207 PBS buffer, samples were dehydrated and then hybridized with smFISH probes. About 20-nt
208 smFISH probes were designed to bind specifically across the length of each target RNA in a non-
209 overlapping series (Markey *et al.*, 2014). For small RNA detection, probes were designed reverse
210 complemented to ~19 nt of the phasiRNA sequences generated from each locus. Briefly, 23-51
211 probes (total coverage of about 800 nt for mRNAs or sRNAs) were designed for each target, and
212 each probe was synthesized with a 3′ amino modification (LGC Biosearch Technologies, CA)
213 (Table **S3**). All the probes of one set were pooled and *en masse* coupled with Alexa Fluor 647
214 (Thermo Fisher) or Texas Red; the labeled probe fraction was purified using reverse phase
215 HPLC (Batish *et al.*, 2011). The probes were diluted to a concentration of 20 ng/µl in a

216 hybridization buffer containing 10% formamide, 1 mg/mL yeast tRNA, 10% dextran sulfate, and
217 2 mM Vanadyl ribonucleoside complex (New England Biolab, Ipswich, MA, Catalogue Number,
218 S142), 0.02% RNase free BSA (Ambion, AM2618). The biological samples were hybridized
219 with probes overnight in a humid chamber at 37°C. The samples were then washed two times
220 with 2X SSC buffer (sodium saline citrate) containing 10% formamide, and a final wash was
221 done using 1X TBS buffer (Tris-buffered saline). Samples were mounted using ProLong™ Glass
222 Antifade Mountant with NucBlue™ Stain (ThermoFisher Scientific, P36981).
223 Fluorescence was detected by spectral unmixing of autofluorescence spectra using laser
224 scanning confocal microscopy on a Zeiss LSM 880 multiphoton confocal microscope. We used
225 30% power of the 633 nm laser and an alpha Plan-Apochromat 100x/1.46 oil lens to acquire
226 RNA *in situ* images. Pure dye was used as positive control, and autofluorescence from maize
227 tissue was used as the negative control for spectral bleed-through. After images were acquired,
228 each image was spectra unmixed. The brightness and contrast of images in the same figure panel
229 were adjusted equally and linearly in Zen 2010 (Carl Zeiss). For quantification, the numbers for
230 each localization event were calculated using ImageJ (SpotQuant). Two replicates for each Z-
231 stack of images were used for calculating the copy number for each gene's transcripts.
232
233 **Results**
234 **LCM collections from meiotic stage maize anthers**
235 Control of fertility in maize anthers, the male reproductive floral organs, is important for hybrid
236 seed production as an economic way to improve grain yield. Maize tassels produce hundreds of
237 spikelets, each of which contains an upper and lower floret, and each floret contains three anthers
238 (Fig. **1a**). The lower floret stamens develop approximately 1 day later than the upper floret
239 stamens within the same spikelet. At the beginning of meiosis, each anther contains four lobes;
240 each lobe consists of four somatic cell types that are required to support meiotic cell
241 development (Fig. **1a**). The high regularity of maize anther development, numerous anthers, and
242 a detailed staging system allow rapid dissection of carefully staged anthers for cytological and
243 molecular analysis (Fig. **1b, c**) (Kelliher & Walbot, 2011). To explore the spatial distribution of
244 24-nt phasiRNAs and their pathway components in the W23 inbred (Fig. **2a**), LCM was used to
245 isolate three samples (ME, TAP, and OSC) from two stages of meiotic anthers (1.5 mm zygotene
246 and 2.0 mm pachytene) (Fig. **S1**; Table **S4**). Collections from additional stages were used in RT-

247 qPCR analysis to provide finer detail of the timing of biogenesis of a subset of 24-*PHAS*
248 precursor and *Dcl5* transcripts.
249
250 **24-*PHAS* precursors accumulate in tapetal cells**
251 Seventeen RNA-seq libraries were built from ME, TAP, and OSC recovered from 1.5 mm and
252 2.0 mm stage anthers plus single, fixed anthers (FA) (Table **S5**). To check the reproducibility of
253 the datasets, a correlation heatmap and a Principal Component Analysis (PCA) plot were
254 constructed (Fig. **1d, e**). Biological replicates are highly similar and distinct from other cell
255 collections at both stages, confirming the high quality of our LCM sample collections. 126
256 (TPM > 0) of 176 previously discovered 24-*PHAS* precursor types were identified in FA and
257 LCM cell sample collections (Table **S6**) (Zhai *et al.*, 2015); *PHAS* precursors that overlapped
258 protein coding genes were excluded. As shown in Fig. **2b**, 118 of these loci had sufficient and
259 reliable expression (TPM reads > 5 in at least one sample) for further analysis. Overall, the 24-
260 *PHAS* precursors were most abundant in TAP at the 1.5 mm stage, showing an expression
261 pattern and high abundance similar to that in 1.5 mm FA (Fig. **2b**); therefore, the majority of 24-
262 *PHAS* precursors in whole anthers are found in the tapetal cells. The average total expression
263 levels of 24-*PHAS* loci are approximately 65 times lower in ME and 20 times lower in OSC at
264 this zygotene stage (Fig. **2b**; Table **S6**). Single cell RNA-seq (scRNA-seq) analysis of individual
265 ME detected a low abundance of transcripts from 24-*PHAS* loci during the pre-
266 zygotene/zygotene stages in a A188/B73 maize hybrid stock (Nelms & Walbot, 2022),
267 confirmation of low precursor abundance in meiocytes. The total average abundance of these 24-
268 *PHAS* transcripts per zygotene sample in A188/B73 is less than that in the pooled meiocyte LCM
269 samples at 1.5 mm from W23 maize anthers. Furthermore, our previous scRNA-seq data also
270 identified extremely low abundances of 24-*PHAS* precursors in premeiotic AR and PMC in W23
271 maize anthers (Nelms & Walbot, 2019). These data suggests that the TAP is the main source for
272 24-*PHAS* precursors in zygotene stage maize anthers.
273 To further verify our LCM RNA-seq data and to quantify transcripts in more stages, we
274 randomly selected three highly expressed 24-*PHAS* precursors (*PHAS15*, *PHAS116*, and
275 *PHAS296*) for smFISH and RT-qPCR assays (Fig. **2c**). In the LCM RNA-seq data, transcripts for
276 all three loci were significantly enriched in TAP at the 1.5 mm stage compared to ME and OSC
277 (Fig. **S2**). smFISH images confirmed that TAP contained most of these three 24-*PHAS*

278 transcripts (yellow dots resulting from dye AF647 labeling) at the 1.25 mm and 1.5 mm stages
279 during late leptotene/pre-zygotene and zygotene stages in W23 anthers (Fig. **2d, g**, Fig. **S3a**).
280 Quantification counts (transcript count) demonstrated that TAP is significantly higher at both
281 stages (Fig. **2e, h**, Fig. **S3b**). Almost no expression was detected at earlier or later stages (Fig.
282 **2d, e, g, h**, Fig. **S3a**) or in control hybridization assays using probes that should only detect the
283 long precursor transcript (Fig. **S4**). To confirm this assumption, hybridization assays were
284 repeated now including seven probes that overlap sufficiently with product 24-nt small RNAs to
285 detect phasiRNAs from *PHAS15*. The signals for *PHAS15* were highly increased when these
286 seven overlapping probes were included; furthermore, signal was detected in three cell types
287 including expression at the 1.75 mm stage as expected for 24-nt phasiRNAs (Fig. **S3d**). These
288 data further verified that the distinction between 24-nt phasiRNAs and precursors can be
289 discriminated by smFISH using our methods. For RT-qPCR using W23 anthers and LCM
290 samples, *ZmCyanase* was used as the internal reference; it is consistently expressed across all
291 anther stages and is expressed in all cell layers based on smFISH detection (Fig. **S5**) compared to
292 the no label control hybridization test (Fig. **S6**). In conclusion, in 0.75-2.5 mm W23 maize
293 anthers, the expression patterns of the three 24-*PHAS* loci showed a similar pattern, with high
294 expression levels in both 1.25 mm and 1.5 mm anthers and with significant enrichment in TAP
295 compared to ME and OSC (Fig. **2f, i**, Fig. **S3c**).
296 To further solidify the conclusion that TAP is the primary site of 24-*PHAS* transcript
297 biogenesis, we utilized the *dcl5-mu3* mutant. Several *dcl5* mutants have been documented to
298 contain normal 24-*PHAS* precursor levels but lack virtually all the 24-nt phasiRNAs (Teng *et al.*,
299 2020). We reasoned that in the absence of the processing machinery, the large 24-*PHAS*
300 precursors would accumulate in the cells where they were synthesized. This was indeed true as
301 the *PHAS116* transcripts were found to be highly enriched in TAP at the 1.75 mm stage (this is a
302 slightly later stage than in W23 anthers) in homozygous *dcl5* (*dcl5-mu03//dcl5-mu03*) anthers
303 (mixed inbred background) using smFISH (Fig. **2j**).
304 Overall, these data demonstrate that maize tapetal cells are the main site for 24-*PHAS*
305 precursor accumulation and that accumulation starts at early meiotic prophase I and peaks during
306 zygotene. We also established that accumulation is already substantial at the initial stages of
307 meiosis in 1.25 mm anthers, approximately one day earlier than detected previously by analysis
308 of 1.0 mm and 1.5 mm W23 whole anthers (Zhai *et al.*, 2015).

309

310 **The spatial distribution of 24-nt phasiRNA biogenesis pathway components**

311 Argonaute (AGO) proteins, binding partners of miRNAs and phasiRNAs, play essential roles in
312 phasiRNAs biogenesis and RNA silencing (RNAi) (Czech & Hannon, 2011; Ma & Zhang,
313 2018). AGOs are assumed to be involved at two steps in 24-nt phasiRNA biogenesis and
314 function: a specific AGO as the binding protein for the miR2275 trigger and one or several
315 AGOs as the binding proteins for the diverse 24-nt phasiRNAs (Fig. **2a**). We identified
316 transcripts encoding 18 AGO proteins in LCM cell collections (Fig. **3a**). Nine AGO protein
317 transcripts were expressed in one or two cell collections, and the other nine AGO proteins were
318 detected in all three cell collections. None of the AGO isotype transcripts were specific to tapetal
319 cells. Fifteen of 18 AGO members were expressed in TAP at the 1.5 mm stage, providing a list
320 of AGOs that could be involved in 24-nt phasiRNA biogenesis (Fig. **3a**). Among these, AGO1
321 family members have already been designated as candidates in previous studies in maize and rice
322 (Fei *et al.*, 2016; Kakrana *et al.*, 2018; Araki *et al.*, 2020), and now three AGO members
323 (AGO10b, AGO2b, and AGO5c) not expressed in 1.5 mm TAP can likely be excluded as
324 candidates for 24-nt phasiRNA biogenesis (Fig. **3a**). In meiocytes, transcripts were found for 11
325 AGO proteins, many of which were more highly expressed in ME than other cell types, but none
326 were exclusive to ME (Fig. **3a**). Several of these AGO types were predicted in previous
327 transcriptome profiling and spatial localization studies to be potential 24-nt phasiRNA binding
328 partners, such as AGO18 family members (Zhai *et al.*, 2015; Fei *et al.*, 2016; Sun *et al.*, 2019)
329 and AGO2b (Fei *et al.*, 2016) based on the timing of their expression. It is noteworthy that we
330 detected abundant *AGO5c* transcripts, and these were enriched in ME and absent in TAP (Fig.
331 **3a**). AGO5c is encoded by the maize *male-sterile28* gene and is homologous to rice MEL1 (Li *et*
332 *al.*, 2021), which is the binding partner for a subset of 21-nt phasiRNAs in rice (Komiya *et al.*,
333 2014).

334 We investigated the transcript abundance of *Dcl5* and *Rdr6* in the LCM RNA-seq data.
335 *Dcl5* was significantly higher in TAP at the 1.5 mm stage than any other samples (Fig. **3b**). In
336 contrast, *Rdr6* was expressed in all three cell collections, with slightly higher expression levels in
337 ME, followed by TAP at both stages (Fig. **3b**). To precisely pinpoint the timing of expression,
338 RT-qPCR demonstrated that *Dcl5* transcripts were significantly higher in TAP samples (Fig. **3c**);
339 furthermore, the expression pattern of *Dcl5* is similar to the three 24-*PHAS* precursors (*PHAS15*,

340 *PHAS116*, and *PHAS296*), with the highest expression levels detected in TAP compared to ME
341 or OSC at both the 1.25 mm and 1.5 mm stages (Fig. **3c**). As shown in Fig. **3d-f** with smFISH
342 detection, *Dcl5* transcripts (yellow dots resulting from Texas Red labeled smFISH probes) were
343 prominently localized in TAP at the 1.25 mm, 1.5 mm, and 1.75 mm stages in either W23
344 anthers or heterozygous *Dcl5*//*dcl5* fertile anthers. Far fewer yellow dots were detected in ME or
345 OSC, and almost no signal was detected in the negative control samples (Fig. **3f**, Fig. **S6**). An
346 additional smFISH analysis of *Dcl5* using AF647 labeled smFISH probes confirmed that *Dcl5*
347 transcripts were localized mainly in TAP at 1.25 mm and 1.5 mm (Fig. **S7**). These data suggest
348 that TAP is the main site for *Dcl5* accumulation at early meiotic prophase I in maize.
349 Previous studies have reported that four basic helix-loop-helix (bHLH) factors (*Ms23*,
350 *Ms32*, *bHLH52*, and *bHLH122*) are required for normal tapetal cell specification and
351 differentiation in maize (Moon *et al.*, 2013; Nan *et al.*, 2017). *Ms23* is the master transcription
352 factor (TF) and is required for expression of 24-*PHAS* precursors, miR2275, and 24-nt
353 phasiRNAs (Zhai *et al.*, 2015). Here, *Ms23* and *bHLH51* were highly expressed in TAP at 2.0
354 mm, whereas *Ms32* and *bHLH122* were more abundant in TAP at 1.5 mm (Fig. **S8**). These TF
355 expression patterns are consistent with our previous work in maize anthers, particularly the
356 absence of *bHLH122* transcripts at 2.0 mm (Nan *et al.*, 2017). Importantly, the TAP is
357 significantly higher for these four TFs compared with the other two cell collections (Fig. **S8**).
358 Collectively, the distribution of key TFs by RNA-seq and localization data provide further
359 evidence that TAP is the main site for transcription of *PHAS* precursors and their processing into
360 24-nt phasiRNAs. Based on the timing of 24-*PHAS* accumulation, heterodimers of *Ms32* and
361 *bHLH122* are candidates for direct regulation of 24-*PHAS* loci. Because *Ms23* is essential for
362 expression of *bHLH122,* it is also a critical factor.
363
364 **24-nt phasiRNAs are abundant in all three cell collections**
365 To investigate the spatial distribution of 24-nt phasiRNAs in meiotic stage anthers, we collected
366 ME, TAP, and OSC by LCM from 1.5 mm and 2.0 mm W23 maize anthers for low input sRNA-
367 seq (Table **S4**, Table **S5**). We first classified sRNAs by length (18 nt to 30 nt) in FA and LCM
368 cell collections. Confirming previous results (Zhai *et al.*, 2015), the 24-nt size sRNA class is the
369 most abundant at both stages (Fig. **S9a**). The 21-nt size sRNA class is also detectable, but with
370 lower expression levels (Fig. **S9a**). Using the set of 118 24-*PHAS* loci for analysis (Fig. **2b**), 24-

371 nt phasiRNAs from these loci were more abundant in all three cell collections at 2.0 mm than at
372 the 1.5 mm stage (Fig. **4a**; Table **S6**). The expression patterns of 24-nt phasiRNAs and 22-nt
373 miR2275 family members are very similar, with the highest abundance in ME at 2.0 mm during
374 pachytene, followed by TAP at this stage (Fig. **4a**). A previous sRNA-FISH co-localization study
375 reported that miR2275 and one 24-nt phasiRNA had higher abundances in AR/ME and TAP in
376 maize anthers (Huang *et al.*, 2019). Here, two of the miR2275 family members (miR2275a and
377 miR2275b) were highly expressed, indicating they might play key roles in 24-*PHAS* precursor
378 cleavage (Fig. **4b**). Although the precursors are most abundant in TAP cells (Fig. **2b, c**, Fig. **S2**),
379 the 24-nt phasiRNAs accumulate to higher levels in the ME (Fig. **4a, c**, Fig. **S9b**). Individual 24-
380 nt sRNA abundances from products of the same locus (*PHAS15*, *PHAS116*, and *PHAS296*) are
381 not uniform: only a few of the 24-nt sRNAs show high abundance despite the expectation of
382 equal stoichiometry from a single precursor molecule (Fig. **4d, e**, Fig. **S10a**). Furthermore,
383 sRNAs localization studies illustrated that 24-nt phasiRNAs from three 24-*PHAS* loci (*PHAS15*,
384 *PHAS116*, and *PHAS296*) accumulated in all three cell types, with higher expression levels in
385 ME and TAP, lower in OSC from 1.25 mm to 2.0 mm in W23 anthers (Fig. **4f-h,** Fig. **S10b**).
386 Almost zero expression, considered to be background, was detected in control hybridization
387 assays (*dcl5* mutants, mouse HKH RNA control, and no labeled control) (Fig. **4h**, Fig. **S10c, d**).
388 These distribution patterns lead us to hypothesize that the TAP is the site for nearly all 24-nt
389 phasiRNAs biogenesis and that the presence of 24-nt phasiRNAs in ME and OSC depends on
390 transport during early meiotic prophase I in maize.

391 **Discussion**

392 In anthers, TAP is the innermost of the four somatic layers, adjacent to the germinal cells. The
393 TAP plays essential roles in providing nutrients, enzymes, and pollen wall components to
394 support AR, ME, and microspore (MSP) development. Defects in tapetal function or the
395 abnormal differentiation of TAP usually leads to meiotic arrest or to later pollen abortion (Li *et*
396 *al.*, 2006; Xu *et al.*, 2010; Moon *et al.*, 2013; Niu *et al.*, 2013; Nan *et al.*, 2017; Teng *et al.*,
397 2020). 24-nt phasiRNAs have been reported as abundant in meiotic stage maize anthers from
398 hundreds of unique copy loci (Zhai *et al.*, 2015). In TAP-defective, male-sterile mutants lacking
399 key tapetal-expressed TFs, almost all the 24-nt phasiRNAs are missing (Zhai *et al.*, 2015; Nan *et*
400 *al.*, 2017), which indicates that TAP is likely to be involved in 24-nt phasiRNA biogenesis. Our
401 low-input RNA-seq data for ME, TAP, and OSC demonstrated that the TAP is the main source
402 for the 118 24-*PHAS* precursor transcripts as well as *Dcl5* transcripts in 1.5 mm stage anthers
403 (Fig. **2b, c**, Fig. **3b**), confirming a previous study in the same W23 background that 1.5 mm
404 anthers were the peak stage for 24-*PHAS* loci production with 1.0 mm anthers lacking expression
405 (Zhai *et al.*, 2015). We further refined the timing using smFISH and RT-qPCR assays,
406 demonstrating that three selected 24-*PHAS* loci (*PHAS15*, *PHAS116*, and *PHAS296*) and *Dcl5*
407 transcripts were initially expressed at 1.25 mm during the leptotene-zygotene transition and were
408 continuously expressed at 1.5 mm or 1.75 mm during zygotene (Fig. **2d-i**, Fig. **3d-f**, Fig. **S3**, Fig.
409 **S7**). Moreover, the earlier timing for 24-nt phasiRNA generation corresponds to the stage just
410 prior to and including the leptotene-zygotene transition (Fig. **4f, g**, Fig. **S10b**), which is a key
411 checkpoint in meiosis. A previous study has reported that CHH DNA methylation is elevated in
412 isolated ME, specifically at the phasiRNA-producing loci (Dukowic-Schulze *et al.*, 2016).
413 Therefore, a logical hypothesis is that some of the 24-nt phasiRNAs generated in the TAP and
414 transported to ME might induce methylation in the corresponding loci. It is unclear how such *cis*
415 methylation could contribute to meiotic regulation. Furthermore, in *dcl5* mutants, meiosis is
416 normal in the near complete absence of 24-nt phasiRNAs (Teng *et al.*, 2020), indicating that
417 whatever role the 24-nt phasiRNAs play in meiosis, it is dispensable.

418 By using LCM-purified cell collections, our data demonstrate that TAP cells are the
419 primary site of 24-*PHAS* precursor accumulation and 24-nt phasiRNA biogenesis. sRNA-seq
420 data for ME, TAP, and OSC illustrated that 24-nt phasiRNAs and miR2275 family members
421 were found in all three cell collections, with higher accumulation levels in ME at 2.0 mm during

422 pachytene, followed by TAP at the same stage (Fig. **4a-c**). Furthermore, sRNA-FISH detection
423 confirmed that the 24-nt phasiRNAs originating from three 24-*PHAS* loci (*PHAS15*, *PHAS116*,
424 and *PHAS296*) were present in all three cell layers from 1.25 mm to 2.0 mm (Fig. **4f, g**, Fig.
425 **S10b**). Our major new conclusion is the proposal that 24-nt phasiRNAs generated in the TAP
426 move to other cell types. This conclusion is summarized in a model of 24-phasiRNA biogenesis
427 and mobility in maize anthers during meiotic prophase I (Fig. **5**). We demonstrated that TAP is
428 the main site of 24-nt phasiRNAs biogenesis, as TAP contain the vast majority of 24-*PHAS*
429 precursors, *Dcl5* transcripts, adequate miR2275, and *Rdr6*. To understand why ME later contain
430 the highest levels of 24-nt phasiRNAs, we note that there are approximately 30 tapetal cells
431 touching each ME, whereas only approximately 0.6 tapetal cell touch neighboring OSC (Kelliher
432 & Walbot, 2011). Utilizing the LCM cell numbers we recovered and the total 24-nt phasiRNA
433 reads we generated (Table **S4**, Table **S6**), we calculated that each tapetal cell "donates"
434 approximately 5% of its 24-nt phasiRNAs to ME or OSC during meiotic prophase I in maize
435 anthers. If each TAP cells exports 5% (5 units) of its 24-nt phasiRNAs to ME cells, each ME
436 would have 5 units x 30 = 150 units of 24-nt phasiRNAs, therefore reaching a higher level than
437 the source TAP cells. In contrast, export of 5 units of 24-nt phasiRNAs to the OSC, would result
438 in a low level of 24-nt phasiRNAs in the immediate receiving middle layer cell with further
439 dilution as 24-nt phasiRNAs move throughout the OSC group. A challenge for future research
440 will be documenting the path of 24-nt phasiRNA movement. Other cases of plant intercellular
441 movement of sRNAs are probably through PD, regulating tissue or organ development by gene
442 silencing and RdDM (Dunoyer *et al.*, 2013). PD are membrane-lined intercellular channels that
443 connect the cytoplasms of adjacent cells, such as between TAP and PMC/ME or non-TAP
444 somatic cells in anthers (Mamun *et al.*, 2005; Sager & Lee, 2014). Therefore, we speculate that
445 24-nt phasiRNAs move from the biogenesis site in TAP to ME or OSC through PD in meiotic
446 prophase I maize anthers.
447 In *Arabidopsis*, tapetal-derived 24-nt siRNAs induce DNA methylation in the germline
448 and maintain genome integrity by silencing corresponding genes and transposons (Long *et al.*,
449 2021). Here, 24-nt phasiRNAs are generated in TAP and then exported to ME (Fig. **5**). These
450 exported 24-nt phasiRNAs are likely required for the elevated CHH DNA methylation at 24-
451 *PHAS* loci in isolated ME in maize (Dukowic-Schulze *et al.*, 2016). In *Arabidopsis*, the 24-nt
452 siRNAs appear to have a broader role in modifying the ME genome and gene expression than the

453 24-nt phasiRNAs have in maize. This is particularly true for any impact 24-nt phasiRNAs might
454 have on gene expression, because no mRNA targets for this class of small RNAs have been
455 identified. Nonetheless, it is interesting that small RNAs synthesized in the TAP are transferred
456 to maize ME. Analysis of *dcl5* maize mutants establishes that in the absence of 24-nt phasiRNA
457 biogenesis, tapetal cells fail to differentiate properly at normal maize growing temperatures
458 (28 °C), while meiosis proceeds normally (Teng *et al.*, 2020). These observations indicate that
459 the 24-nt phasiRNAs play an essential role in the TAP -- not in ME -- during the meiotic stages;
460 later, microspore failure renders *dcl5* mutants male-sterile, a fact that we attribute to the failure
461 of the tapetum to supply nutrients and wall components to the developing uninucleate
462 microspores. Mutants grown at low temperature (21 °C) are fertile and tapetal development is
463 slow but sufficient indicating that 24-nt phasiRNAs are not required under these conditions.
464 Considering these observations *in toto,* it is possible that in maize the transfer of 24-nt
465 phasiRNAs to meiocytes is an evolutionary relic that no longer serves (or fully serves) a required
466 function and that the primary role of the 24-nt phasiRNAs is to support rapid tapetal
467 differentiation.

468 **Acknowledgements**
469 We thank M. Zhang for initial suggestions on project design and for instructing X. Zhou in the
470 LCM technique; B. Nelms for help with low input RNA-seq library construction and raw data
471 processing; Y. Chan and Y. Liu for help in data handling; J. Caplan for helpful advice on
472 smFISH; J. Zhan assisted retrieval and organization of the sequences of 24-*PHAS* precursors and
473 24-nt phasiRNAs; and J. Dinneny for use of the SP8 confocal microscope. This research was
474 supported by National Science Foundation award 17540974. Requests for materials should be
475 addressed to walbot@stanford.edu.
476
477 **Author Contributions**
478 X.Z., B.C.M., and V.W. conceived and designed the project. X.Z. performed most of the
479 experiments and bioinformatics. K.H. and M.B. designed and synthesized smFISH probes. K.H.,
480 M.B., A.A., T.K., and T.C. performed smFISH and imaging analysis. T.C. constructed sRNA
481 libraries and performed raw data processing. X.Z. and V.W. wrote the manuscript with editing
482 by B.C.M. and K.H. and with contributions from all co-authors.
483
484 **Data Availability**
485 Sequencing data were deposited to the Gene Expression Omnibus (accession no. GSE182588 for
486 RNA-seq data; accession no. GSE182476 for sRNA-seq data) and will be made public after peer
487 review.
488
489 **Competing interests**
490 The authors declare no competing interests.

491 **Reference**

492 **Araki S, Le NT, Koizumi K, Villar-Briones A, Nonomura KI, Endo M, Inoue H, Saze H,**
493 **Komiya R. 2020.** miR2118-dependent U-rich phasiRNA production in rice anther wall
494 development. *Nat Commun* **11**: 3115.

495 **Aronesty E. 2013.** Comparison of sequencing utility programs. *The open bioinformatics journal*
496 **7**: 1-8.

497 **Batish M, Raj A, Tyagi S. 2011.** Single molecule imaging of RNA in situ. *Methods Mol Biol*
498 **714**: 3-13.

499 **Bolger AM, Lohse M, Usadel B. 2014.** Trimmomatic: a flexible trimmer for Illumina sequence
500 data. *Bioinformatics* **30**: 2114-2120.

501 **Chen S, Zhou Y, Chen Y, Gu J. 2018.** fastp: an ultra-fast all-in-one FASTQ preprocessor.
502 *Bioinformatics* **34**: i884-i890.

503 **Chitwood DH, Timmermans MC. 2010.** Small RNAs are on the move. *Nature* **467**: 415-419.

504 **Czech B, Hannon GJ. 2011.** Small RNA sorting: matchmaking for Argonautes. *Nat Rev Genet*
505 **12**: 19-31.

506 **Dawe RK, Sedat JW, Agard DA, Cande WZ. 1994.** Meiotic chromosome pairing in maize is
507 associated with a novel chromatin organization. *Cell* **76**: 901-912.

508 **Dukowic-Schulze S, Sundararajan A, Ramaraj T, Kianian S, Pawlowski WP, Mudge J,**
509 **Chen C. 2016.** Novel meiotic miRNAs and indications for a role of phasiRNAs in
510 meiosis. *Front Plant Sci* **7**: 762.

511 **Dunoyer P, Melnyk C, Molnar A, Slotkin RK. 2013.** Plant mobile small RNAs. *Cold Spring*
512 *Harb Perspect Biol* **5:** a017807..

513 **Dunoyer P, Schott G, Himber C, Meyer D, Takeda A, Carrington JC, Voinnet O. 2010.**
514 Small RNA duplexes function as mobile silencing signals between plant cells. *Science*
515 **328**: 912-916.

516 **Fan Y, Yang J, Mathioni SM, Yu J, Shen J, Yang X, Wang L, Zhang Q, Cai Z, Xu C, et al.**
517 **2016.** PMS1T, producing phased small-interfering RNAs, regulates photoperiod-sensitive
518 male sterility in rice. *Proc Natl Acad Sci U S A* **113**: 15144-15149.

519 **Fei Q, Yang L, Liang W, Zhang D, Meyers BC. 2016.** Dynamic changes of small RNAs in
520 rice spikelet development reveal specialized reproductive phasiRNA pathways. *J Exp Bot*
521 **67**: 6037-6049.

522 **Hashimshony T, Senderovich N, Avital G, Klochendler A, de Leeuw Y, Anavy L, Gennert**
523 **D, Li S, Livak KJ, Rozenblatt-Rosen O, et al. 2016.** CEL-Seq2: sensitive highly-
524 multiplexed single-cell RNA-Seq. *Genome Biol* **17**: 77.
525 **Huang K, Baldrich P, Meyers BC, Caplan JL. 2019.** sRNA-FISH: versatile fluorescent in situ
526 detection of small RNAs in plants. *Plant J* **98**: 359-369.
527 **Johnson C, Kasprzewska A, Tennessen K, Fernandes J, Nan GL, Walbot V, Sundaresan V,**
528 **Vance V, Bowman LH. 2009.** Clusters and superclusters of phased small RNAs in the
529 developing inflorescence of rice. *Genome Res* **19**: 1429-1440.
530 **Kakrana A, Mathioni SM, Huang K, Hammond R, Vandivier L, Patel P, Arikit S,**
531 **Shevchenko O, Harkess AE, Kingham B, et al. 2018.** Plant 24-nt reproductive
532 phasiRNAs from intramolecular duplex mRNAs in diverse monocots. *Genome Res* **28**:
533 1333-1344.
534 **Kelliher T, Walbot V. 2011.** Emergence and patterning of the five cell types of the Zea mays
535 anther locule. *Dev Biol* **350**: 32-49.
536 **Kelliher T, Walbot V. 2012.** Hypoxia triggers meiotic fate acquisition in maize. *Science* **337**:
537 345-348.
538 **Kersey PJ, Allen JE, Armean I, Boddu S, Bolt BJ, Carvalho-Silva D, Christensen M, Davis**
539 **P, Falin LJ, Grabmueller C, et al. 2016.** Ensembl Genomes 2016: more genomes, more
540 complexity. *Nucleic Acids Res* **44**: D574-580.
541 **Kivioja T, Vaharautio A, Karlsson K, Bonke M, Enge M, Linnarsson S, Taipale J. 2011.**
542 Counting absolute numbers of molecules using unique molecular identifiers. *Nat Methods*
543 **9**: 72-74.
544 **Komiya R, Ohyanagi H, Niihama M, Watanabe T, Nakano M, Kurata N, Nonomura K.**
545 **2014.** Rice germline-specific Argonaute MEL1 protein binds to phasiRNAs generated
546 from more than 700 lincRNAs. *Plant J* **78**: 385-397.
547 **Li N, Zhang DS, Liu HS, Yin CS, Li XX, Liang WQ, Yuan Z, Xu B, Chu HW, Wang J, et**
548 **al. 2006.** The rice tapetum degeneration retardation gene is required for tapetum
549 degradation and anther development. *Plant Cell* **18**: 2999-3014.
550 **Li Y, Huang Y, Pan L, Zhao Y, Huang W, Jin W. 2021.** Male sterile 28 encodes an
551 ARGONAUTE family protein essential for male fertility in maize. *Chromosome Res* **29**:
552 189-201.

553 **Long J, Walker J, She W, Aldridge B, Gao H, Deans S, Vickers M, Feng X. 2021.** Nurse
554 cell-derived small RNAs define paternal epigenetic inheritance in Arabidopsis. *Science*
555 **373**: eabh0556.
556 **Ma Z, Zhang X. 2018.** Actions of plant Argonautes: predictable or unpredictable? *Curr Opin*
557 *Plant Biol* **45**: 59-67.
558 **Mamun EA, Cantrill LC, Overall RL, Sutton BG. 2005.** Cellular organisation in meiotic and
559 early post-meiotic rice anthers. *Cell Biol Int* **29**: 903-913.
560 **Markey FB, Ruezinsky W, Tyagi S, Batish M. 2014.** Fusion FISH imaging: single-molecule
561 detection of gene fusion transcripts in situ. *PLoS One* **9**: e93488.
562 **Mathioni SM, Kakrana A, Meyers BC. 2017.** Characterization of Plant Small RNAs by Next
563 Generation Sequencing. *Curr Protoc Plant Biol* **2**: 39-63.
564 **Molnar A, Melnyk CW, Bassett A, Hardcastle TJ, Dunn R, Baulcombe DC. 2010.** Small
565 silencing RNAs in plants are mobile and direct epigenetic modification in recipient cells.
566 *Science* **328**: 872-875.
567 **Moon J, Skibbe D, Timofejeva L, Wang CJ, Kelliher T, Kremling K, Walbot V, Cande**
568 **WZ. 2013.** Regulation of cell divisions and differentiation by MALE STERILITY32 is
569 required for anther development in maize. *Plant J* **76**: 592-602.
570 **Nan GL, Zhai J, Arikit S, Morrow D, Fernandes J, Mai L, Nguyen N, Meyers BC, Walbot**
571 **V. 2017.** MS23, a master basic helix-loop-helix factor, regulates the specification and
572 development of the tapetum in maize. *Development* **144**: 163-172.
573 **Nelms B, Walbot V. 2019.** Defining the developmental program leading to meiosis in maize.
574 *Science* **364**: 52-56.
575 **Nelms B, Walbot V. 2022.** Gametophyte genome activation occurs at pollen mitosis I in maize.
576 **Science** 375: 424-429.
577 **Niu N, Liang W, Yang X, Jin W, Wilson ZA, Hu J, Zhang D. 2013.** EAT1 promotes tapetal
578 cell death by regulating aspartic proteases during male reproductive development in rice.
579 *Nat Commun* **4**: 1445.
580 **Patel P, Mathioni SM, Hammond R, Harkess AE, Kakrana A, Arikit S, Dusia A, Meyers**
581 **BC. 2021.** Reproductive phasiRNA loci and DICER-LIKE5, but not microRNA loci,
582 diversified in monocotyledonous plants. *Plant Physiol* **185**: 1764-1782.

583 **Pertea M, Kim D, Pertea GM, Leek JT, Salzberg SL. 2016.** Transcript-level expression
584 analysis of RNA-seq experiments with HISAT, StringTie and Ballgown. *Nature*
585 *protocols* **11**: 1650-1667.
586 **Pokhrel S, Huang KC, Meyers BC. 2021.** Conserved and non-conserved triggers of 24-nt
587 reproductive phasiRNAs in eudicots. *Plant J* **107:** 1332-1345.
588 **Sager R, Lee JY. 2014.** Plasmodesmata in integrated cell signalling: insights from development
589 and environmental signals and stresses. *J Exp Bot* **65**: 6337-6358.
590 **Schneider CA, Rasband WS, Eliceiri KW. 2012.** NIH Image to ImageJ: 25 years of image
591 analysis. *Nat Methods* **9**: 671-675.
592 **Song X, Li P, Zhai J, Zhou M, Ma L, Liu B, Jeong DH, Nakano M, Cao S, Liu C, et al.**
593 **2012a.** Roles of DCL4 and DCL3b in rice phased small RNA biogenesis. *Plant J* **69**:
594 462-474.
595 **Song X, Wang D, Ma L, Chen Z, Li P, Cui X, Liu C, Cao S, Chu C, Tao Y, et al. 2012b.**
596 Rice RNA-dependent RNA polymerase 6 acts in small RNA biogenesis and spikelet
597 development. *Plant J* **71**: 378-389.
598 **Sun W, Chen D, Xue Y, Zhai L, Zhang D, Cao Z, Liu L, Cheng C, Zhang Y, Zhang Z.**
599 **2019.** Genome-wide identification of AGO18b-bound miRNAs and phasiRNAs in maize
600 by cRIP-seq. *BMC Genomics* **20**: 656.
601 **Tamim S, Cai Z, Mathioni SM, Zhai J, Teng C, Zhang Q, Meyers BC. 2018.** Cis-directed
602 cleavage and nonstoichiometric abundances of 21-nucleotide reproductive phased small
603 interfering RNAs in grasses. *New Phytol* **220**: 865-877.
604 **Tello-Ruiz MK, Naithani S, Stein JC, Gupta P, Campbell M, Olson A, Wei S, Preece J,**
605 **Geniza MJ, Jiao Y, et al. 2018.** Gramene 2018: unifying comparative genomics and
606 pathway resources for plant research. *Nucleic Acids Res* **46**: D1181-D1189.
607 **Teng C, Zhang H, Hammond R, Huang K, Meyers BC, Walbot V. 2020.** *Dicer-like 5*
608 deficiency confers temperature-sensitive male sterility in maize. *Nat Commun* **11**: 2912.
609 **Xia R, Chen C, Pokhrel S, Ma W, Huang K, Patel P, Wang F, Xu J, Liu Z, Li J, et al. 2019.**
610 24-nt reproductive phasiRNAs are broadly present in angiosperms. *Nat Commun* **10**: 627.
611 **Xu J, Yang C, Yuan Z, Zhang D, Gondwe MY, Ding Z, Liang W, Zhang D, Wilson ZA.**
612 **2010.** The ABORTED MICROSPORES regulatory network is required for postmeiotic
613 male reproductive development in *Arabidopsis thaliana*. *Plant Cell* **22**: 91-107.

614 **Yadava P, Tamim S, Zhang H, Teng C, Zhou X, Meyers BC, Walbot V. 2021.**
615 Transgenerational conditioned male fertility of HD-ZIP IV transcription factor mutant
616 *ocl4*: impact on 21-nt phasiRNA accumulation in pre-meiotic maize anthers. *Plant*
617 *Reprod* **34**: 117-129.
618 **Yang X, You C, Wang X, Gao L, Mo B, Liu L, Chen X. 2021.** Widespread occurrence of
619 microRNA-mediated target cleavage on membrane-bound polysomes. *Genome Biol* **22**:
620 15.
621 **Zhai J, Zhang H, Arikit S, Huang K, Nan GL, Walbot V, Meyers BC. 2015.**
622 Spatiotemporally dynamic, cell-type-dependent premeiotic and meiotic phasiRNAs in
623 maize anthers. *Proc Natl Acad Sci U S A* **112**: 3146-3151.
624 **Zhang M, Ma X, Wang C, Li Q, Meyers BC, Springer NM, Walbot V. 2021.** CHH DNA
625 methylation increases at 24-PHAS loci depend on 24-nt phased small interfering RNAs in
626 maize meiotic anthers. *New Phytol* **229**: 2984-2997.
627

628 **Figure Legends**

629 **Fig. 1 Staging of maize anthers and quality evaluation of LCM cell sample collections.**
630 (**a**) Male inflorescence structures. From left to right: maize tassel; central spike; single spikelet;
631 three lower and three larger upper florets; transverse confocal microscopy view of a single anther
632 (near the start of meiosis). (**b**) The timeline of maize anther development from initial cell
633 specification, proliferation, and differentiation to pollen maturation. Approximately 10 days of
634 development occur between anther initiation and the start of meiosis at 1.2 mm; meiosis requires
635 6 days and finishes at 2.5 mm with the tetrad stage; an additional 15-16 days are required for
636 microspore and then trinucleate pollen development (note that this portion of the timeline is not
637 drawn to scale), followed by pollen maturation and anthesis after 5 more days. Tracings of
638 confocal images of single anther lobes are shown through the dyad stage. The germinal cell
639 stages are abbreviated as follows: mitotic archesporial cells (AR); post-mitotic pollen mother
640 cells (PMC); meiocytes (ME); uninucleate microspore (UM); binucleate microspore (BM); and
641 mature pollen (MP). (**c**) Fluorescence microscopy images of germinal cells visualized with
642 Hoechst staining. During the meiotic proliferation period (0.75 mm anther), archesporial cells
643 have a central nucleolus (N) and a smaller volume than meiotic nuclei. At premeiotic interphase/
644 early leptotene, the knobs (arrowhead) are round, the nucleoli are located centrally, and
645 chromatin threads are not visible or visible only as localized patches. During leptotene leading to
646 pre-zygotene, the spherical knobs become elongated (arrowhead) coincident with nucleolar
647 movement to the periphery. During zygotene, the knobs are paired (red dashed oval);
648 chromosomes are observed as condensation proceeds. Fully paired bivalents (4 strands per
649 thread) and finally a centrally located nucleolus were observed at pachytene. Scale bar represents
650 2 μm. (**d**) Sample-sample correlation analysis in fixed anthers and LCM cell sample collections
651 at the 1.5 mm and 2.0 mm stages. As shown in the heatmap, the biological replicates of the same
652 sample type are highly correlated at both stages. The scale based on the Pearson correlation is
653 from lightest (no correlation) to darkest (1.0 correlation). Abbreviations: fixed anthers (FA);
654 meiocytes (ME); tapetum (TAP); and other somatic cells (OSC). (**e**) Principal component
655 analysis (PCA) to evaluate the similarity of biological replicates.

656 **Fig. 2 24-*PHAS* precursor distribution in maize anthers.**
657 (**a**) 24-nt phasiRNA biogenesis pathway. miR2275 is complementary to a conserved motif in
658 precursors, resulting in precise cleavage; cleaved products are converted to double stranded
659 molecules by RNA-dependent RNA polymerase 6 (RDR6). Unknown Argonaute (AGO)
660 proteins participate in biogenesis and bind at least a subset of the 24-nt phasiRNA products. (**b**)
661 Heat map depicting the abundances of 118 24-*PHAS* precursors (TPM > 5 in at least one sample)
662 in fixed anthers and LCM cells. Solid bubbles on the left represent the total abundance of 24-
663 *PHAS* precursors in that sample. (**c**) Boxplot depicts the distribution of the 20 most abundant 24-
664 *PHAS* precursors in LCM cell collections. Arrowheads point to the three 24-*PHAS* loci
665 (*PHAS15*, *PHAS116*, and *PHAS296*) chosen to represent different abundances for RT-qPCR and
666 single-molecule FISH (smFISH) verifications. (**d**) and (**g**) smFISH was performed using probes
667 conjugated with dye Alexa Fluor 647 (AF647) against *PHAS116* and *PHAS296* in W23 maize
668 anthers (1.0-2.0 mm). The fluorescent micrographs were taken using laser scanning confocal
669 microscopy. Below the images are enlargements of area in red rectangles. Yellow smFISH spots
670 correspond to precursor transcripts, which primarily accumulate in TAP. Scale bars = 10 μm. (**e**)
671 and (**h**) Quantification analysis of images in (**d**) and (**g**). Transcript counts show the binding
672 events for each cell type at different anther stages using spot count in ImageJ. Two biological
673 and three technical replicates were performed for each stage. Statistical analysis was performed
674 with Prism 8 software. *P* values were determined using one-way ANOVA and Tukey tests.
675 Differences among three cell sample collections within the same anther stage were considered
676 significant for *P* values ≤ 0.05 (* $P \leq 0.05$; ** $P \leq 0.01$; *** $P \leq 0.001$; **** $P \leq 0.0001$). (**f**) and
677 (**I**) Quantification of localization of *PHAS116* and *PHAS296* in whole anthers (0.75- 2.5 mm)
678 and LCM cells (1.25 and 1.5 mm) by RT-qPCR. The expression patterns of these 24-*PHAS*
679 precursors are very similar, with high expression levels in tapetum at 1.25 mm, with a peak at the
680 1.5 mm stage. The tapetal cell sample is significantly higher than either meiocytes or other
681 somatic cells. *P* values were determined using one-way ANOVA and Tukey tests in Prism 8
682 software. Differences among the samples were considered significant for *P* values ≤ 0.05 (* $P \leq$
683 0.05; ** $P \leq 0.01$; *** $P \leq 0.001$; **** $P \leq 0.0001$). Note that there is a different scale for each
684 locus. The reference gene (*ZmCyanase*) was used to normalize expression for the accurate
685 assessment of target *24-PHAS* locus expression. (**j**) smFISH detection of *PHAS116* in
686 homozygous *dcl5-mu03//dcl5-mu03* anthers. The red boxes labeled I and II are enlarged in the

687 adjacent image to the right. No signal was detected in control hybridization assays (*Dcl5* probes)
688 at 1.75 mm stage anthers. Scale bars = 10 μm.

689 **Fig. 3 Evaluation of Argonaute, *Dcl5*, and *Rdr6* expression and *Dcl5* transcript localization**
690 **in maize anthers.**
691 (**a**) RNA abundance from the 18 maize loci encoding Argonaute (AGO) proteins. At least one
692 AGO participates in phasiRNA biogenesis by binding miR2275 and a few others have been
693 shown to bind 24-nt phasiRNAs (see text). (**b**) Transcript abundances in LCM cells for two
694 biogenesis genes from RNA-seq datasets. *Dcl5* was highly expressed in 1.5 mm TAP, and *Rdr6*
695 was enriched in both ME and TAP. Differences among the LCM cell samples were considered
696 significant for P values ≤ 0.05 (** $P \leq 0.01$; *** $P \leq 0.001$) using one-way ANOVA followed by
697 Tukey tests. (**c**) RT-qPCR analysis for *Dcl5* at multiple anther stages and in LCM cell samples.
698 The tapetal cell samples are significantly higher than ME and OSC (** $P \leq 0.01$). Note that each
699 graph has a different scale. (**d**-**e**) smFISH detection and quantification analysis for *Dcl5*
700 transcripts in W23 maize anthers (1.0-2.0 mm). Probes are conjugated with Texas Red dye. The
701 images below each panel are the enlarged portions of red rectangle areas. Yellow smFISH spots
702 correspond to *Dcl5* transcripts are significantly higher in TAP (*** $P \leq 0.001$). Scale bars = 10
703 μm. (**f**) smFISH detection of *Dcl5* transcripts in homozygous *dcl5-mu03//dcl5-mu03* anthers.
704 Probes are conjugated with Texas Red dye. The red boxes designated as I and II indicate the area
705 enlarged in the adjacent image. To validate the lack of *Dcl5* transcripts, no signal was detected in
706 a control hybridization assay utilizing *Dcl5* probes applied to homozygous *dcl5-mu03//dcl5-*
707 *mu03* anthers. Scale bars = 10 μm.

708 **Fig. 4 24-nt phasiRNA distribution in maize anthers.**

709 (**a**) Heat map depicting 24-nt phasiRNA abundance from 118 24-*PHAS* loci in fixed anthers and
710 LCM cell sample collections. Solid bubbles on the left represent the total abundance of miR2275
711 family members and 24-nt phasiRNAs in that sample. The highest levels of 24-nt phasiRNAs
712 and miR2275 family members are in 2.0 mm meiocytes, followed by tapetum at this stage. (**b**)
713 The abundance of miR2275 family members in three LCM cell sample collections. (**c**) Box plot
714 depicting the distribution of 24-nt phasiRNAs from the 20 most abundant 24-*PHAS* loci (same as
715 panel **2c**). (**d-e**) 24-nt sRNA distributions from *PHAS116* and *PHAS296* in FA and LCM cells.
716 The dotted lines represent the miR2275 cleavage sites, and each of the grid lines are spaced 24-
717 nucleotide apart. The accumulation of 24-nt sRNA fragments generated from the same locus are
718 not uniform: only a few of the 24-nt sRNAs show high abundance despite the expectation of
719 equal stoichiometry from a single precursor molecule (Zhang *et al.*, 2021). Overall, accumulation
720 patterns are similar in fixed anthers and LCM cells at each locus. (**f**) 24-nt phasiRNA localization
721 from *PHAS116* in W23 maize anthers (1.25-2.0 mm). Probes are conjugated with Texas Red dye.
722 The red box in each image is enlarged in the panel immediately below each image. Yellow
723 smFISH spots corresponding to 24-nt phasiRNAs are expressed in all three cell types. Scale bars
724 = 10 μm. (**g**) 24-nt phasiRNA localization from *PHAS296* in W23 maize anthers (1.25-1.75 mm).
725 Probes are conjugated with Texas Red dye. The red box in each image is enlarged in the panel
726 immediately below each image. Yellow smFISH spots corresponding to 24-nt phasiRNAs are
727 expressed in all three cell types. No signal was detected in an unlabeled control hybridization.
728 Scale bars = 10 μm. (**h**) 24-nt phasiRNA localization from *PHAS116* in homozygous *dcl5-*
729 *mu03//dcl5-mu03* anthers and W23 maize anthers at the 1.75 mm stage. Probes are conjugated
730 with Texas Red dye. Low to zero signal was detected in negative control images with probes
731 against mouse Hexokinase H (HKH) RNA (negative control). Scale bars = 10 μm.
732

733 **Fig. 5 Model of 24-nt phasiRNAs biogenesis and mobility in maize anthers.**
734 On the left is a colorized confocal image as a transverse section of a single anther. On the right is
735 an enlargement of a portion of a single lobe using the same color scheme. During the leptotene-
736 zygotene transition, 24-nt phasiRNAs are generated in TAP and are proposed to move to other
737 cell types. The 30 TAP cells in contact with each meiocyte are proposed to each export a small
738 fraction of their 24-nt phasiRNAs to ME; similarly, a small amount of TAP 24-nt phasiRNA is
739 exported to first to the adjacent Middle Layer (ML) and then distributed to other OSC.

740 **Supporting Information**

741 **Fig. S1** Sequential application of LCM to isolate ME, TAP, and OSC in 1.5 mm and 2.0 mm
742 W23 anthers.

743 **Fig. S2** Transcript abundances of three *24-PHAS* loci (*PHAS15*, *PHAS116*, and *PHAS296*) in
744 LCM cell sample collections in RNA-seq data.

745 **Fig. S3** *PHAS15* localization in maize anthers.

746 **Fig. S4** Negative control hybridization assay.

747 **Fig. S5** *ZmCyanase* localization in maize anthers.

748 **Fig. S6** No labeled control hybridization assay.

749 **Fig. S7** *Dcl5* localization in maize anthers.

750 **Fig. S8** The distribution of four tapetal-enriched TFs (*Ms23*, *Ms32*, *bHLH51*, and *bHLH122*) in
751 LCM cell sample collections at 1.5 mm and 2.0 mm in the RNA-seq dataset.

752 **Fig. S9** sRNA distribution in maize anthers.

753 **Fig. S10** 24-nt phasiRNAs localization in maize anthers.

754

755 **Table S1** Primer sequences for CEL-seq 2 library preparation.

756 **Table S2** Primer sequences for RT-qPCR by the TaqMan assay.

757 **Table S3** Probes sequences (5'-> 3') used for smFISH or sRNA-FISH.

758 **Table S4** List of LCM cell sample collections from 1.5 mm and 2.0 mm maize anthers.

759 **Table S5** Summary of RNA-seq and sRNA-seq libraries prepared from FA and LCM cell sample
760 collections.

761 **Table S6** Coordinates and abundance of the 126 24-*PHAS* loci and their corresponding 24-nt
762 phasiRNAs in FA and LCM cells.

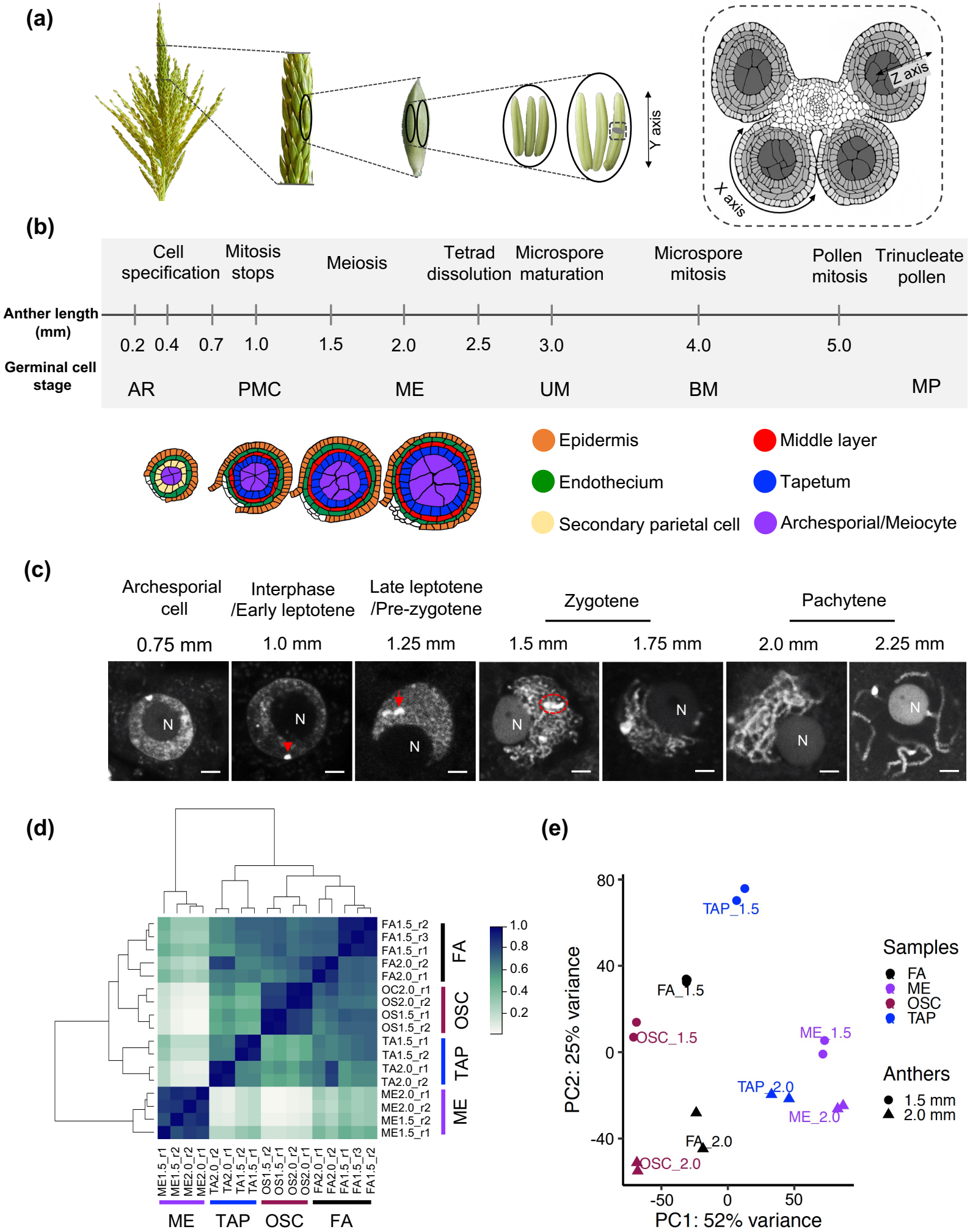

Fig. 1 Staging of maize anthers and quality evaluation of LCM cell sample collections.

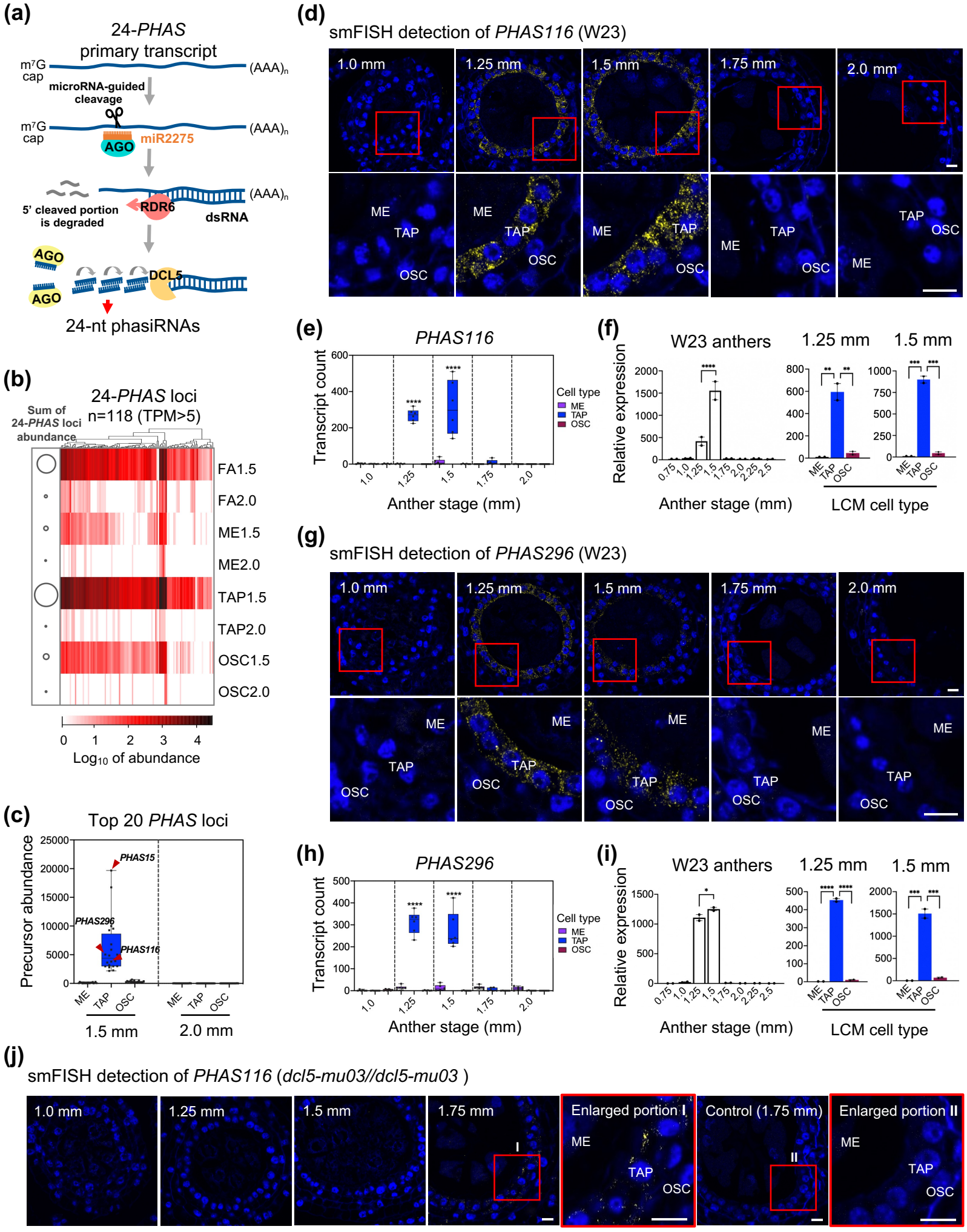

Fig. 2 24-*PHAS* precursor distribution in maize anthers.

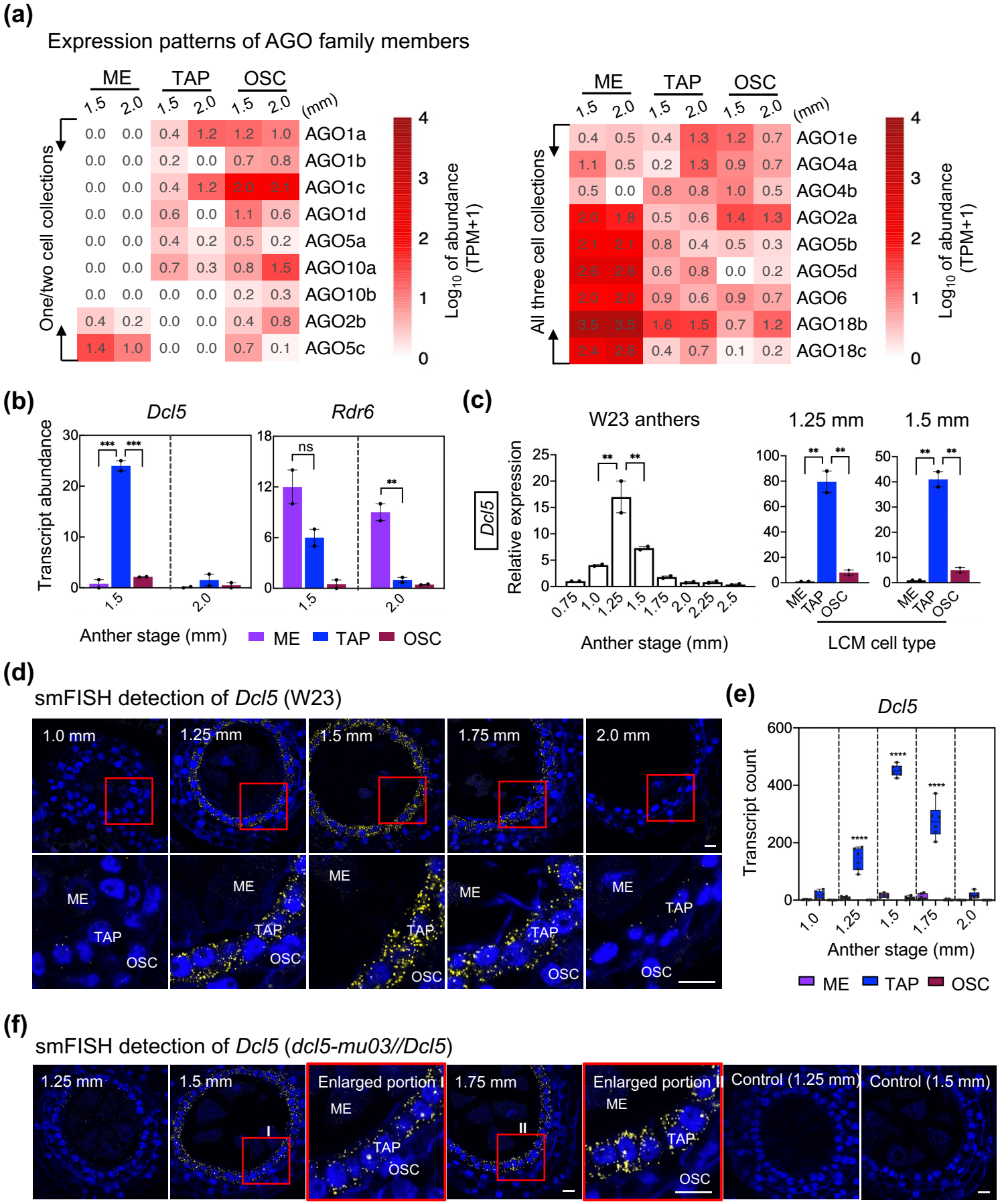

Fig. 3 Evaluation of Argonaute, *Dcl5*, and *Rdr6* expression and *Dcl5* transcript localization in maize anthers.

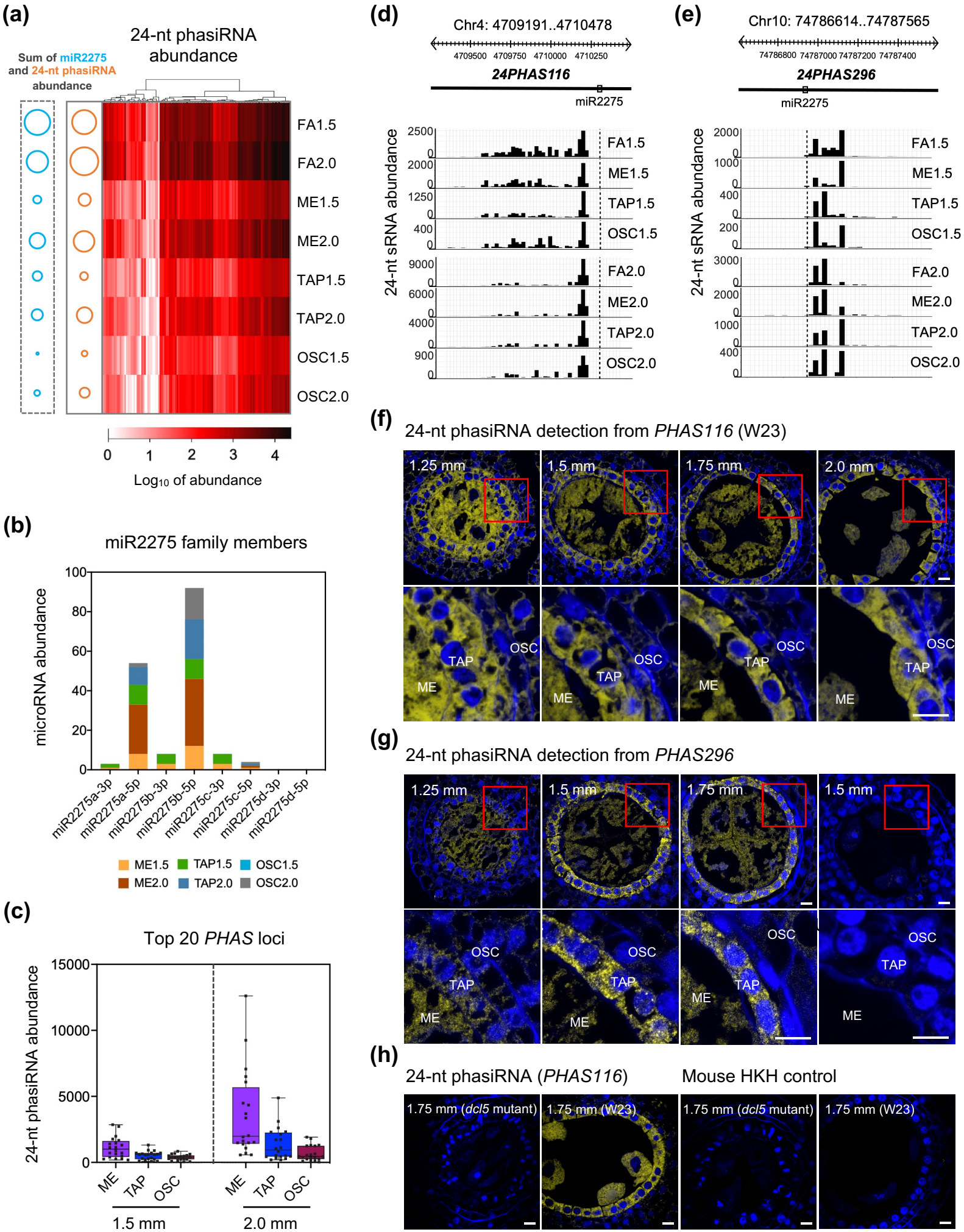

Fig. 4. 24-nt phasiRNA distribution in maize anthers.

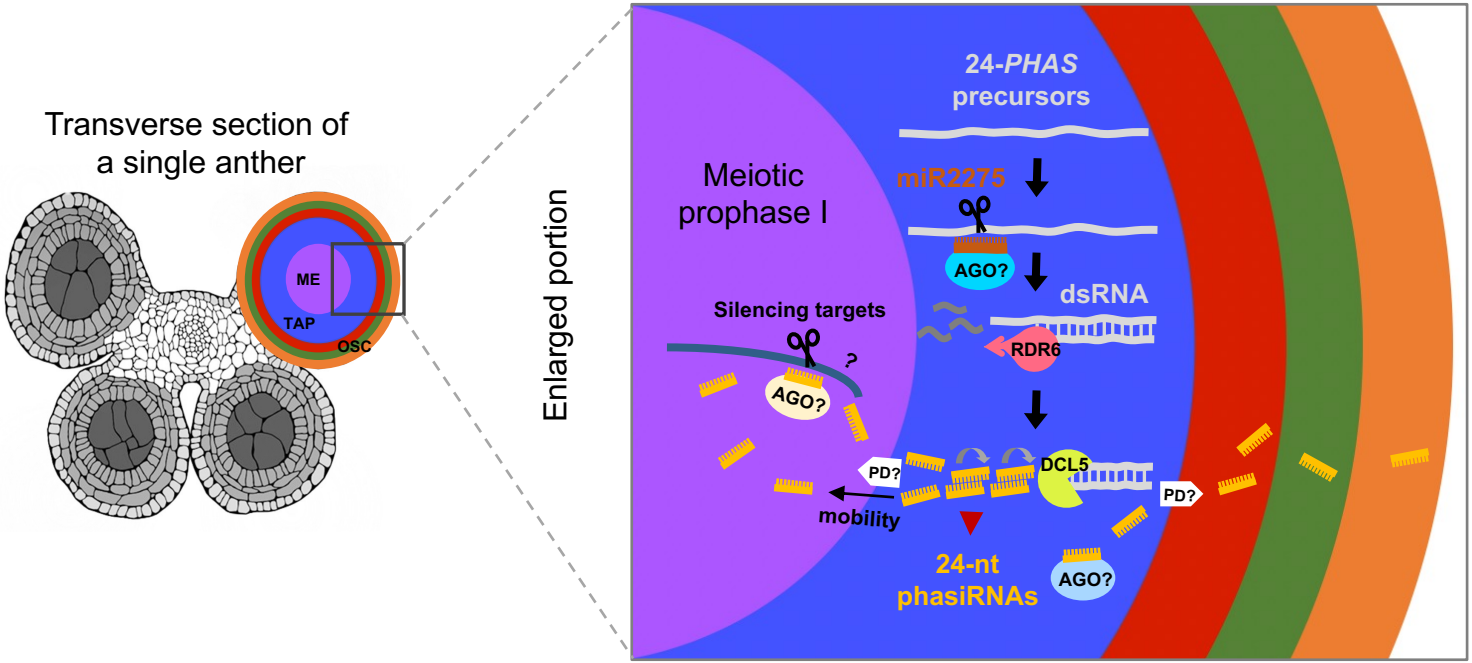

Fig. 5. Model of 24-nt phasiRNAs biogenesis and mobility in maize anthers.